Anomalous losses of energetic particles in the presence of an oscillating radial electric field in fusion plasmas

David Zarzoso, Diego Del-Castillo-Negrete

Anomalous losses of energetic particles in the presence of an oscillating radial electric field in fusion plasmas

David Zarzoso[1]† and Diego del-Castillo-Negrete[2]

[1]Aix-Marseille Université, CNRS, PIIM, UMR 7345 Marseille, France
[2]Oak Ridge National Laboratory, Oak Ridge, TN 37831-8071, United States of America

(Received xx; revised xx; accepted xx)

The confinement of energetic particles in nuclear fusion devices is studied in the presence of an oscillating radial electric field and an axi-symmetric magnetic equilibrium. It is shown that, despite the poloidal and toroidal symmetries, initially integrable orbits turn into chaotic regions that can potentially intercept the wall of the tokamak, leading to particle losses. It is observed that the losses exhibit algebraic time decay different from the expected exponential decay characteristic of radial diffusive transport. A dynamical explanation of this behaviour is presented, within the Continuous Time Random Walk theory. The central point of the analysis is based on the fact that, contrary to the radial displacement, the poloidal angle is not bounded and proper statistical analysis can therefore be made, showing for the first time that energetic particle transport can be super-diffusive in the poloidal direction and characterised by asymmetric poloidal displacement. The connection between poloidal and radial positions ensured by the conservation of the toroidal canonical momentum, implies that energetic particles spend statistically more time in the inner region of the tokamak than in the outer one, which explains the observed algebraic decay. This indicates that energetic particles might be efficiently slowed down by the thermal population before leaving the system. Also, the asymmetric transport reveals a new possible mechanism of self-generation of momentum.

1. Introduction and motivation

Energetic particles (EP) are ubiquitous in both laboratory and astrophysical plasmas. By definition, they exhibit velocities much larger than the thermal velocity of the bulk plasma, which is characterised by a Maxwellian distribution function. EP, such as the alpha particles, must be sufficiently well confined in order to transfer their energy to the bulk plasma through Coulomb collisions or to ensure the current drive efficiency (Heidbrink & Sadler 1994; Pinches *et al.* 2004; Sharapov *et al.* 2000). Nevertheless, due to the curvature of the magnetic field lines, the trajectories of particles depart from the magnetic flux surfaces. This departure (called *magnetic drift*) is more pronounced when the energy of particles increases. Therefore, the magnetic drift of EP can be intense enough so that their trajectories intercept the wall even with circular concentric magnetic surfaces, leading to losses and limiting the performance of the machine. In addition, the presence of a substantial population of particles at high energies leads to gradients in phase space, which may result in instabilities called energetic particle modes (EPM) (see for instance (Chen & Zonca 2007, 2016; Heidbrink 2008; Lauber 2013) and references therein). EPM tend to increase the transport of energetic particles, reducing inevitably

† Email address for correspondence: david.zarzoso-fernandez@univ-amu.fr

the tokamak performance. Therefore, understanding and controlling the EPMs is also of prime importance for the future of ITER. In the presence of fluctuations driven by EP, such as for Toroidal Alfvén Eigenmodes, zonal structures can be nonlinearly generated (Chen & Zonca 2012). Direct excitation of zonal structures by EP is also possible, which occurs in the context of a special class of EPMs called energetic geodesic acoustic modes (EGAMs), dominated by a zonal structure $(m, n) = (0, 0)$ oscillating roughly at the acoustic frequency (Fu 2008; Nazikian *et al.* 2008; Qiu *et al.* 2010; Zarzoso *et al.* 2012). Because EGAMs are axi-symmetric modes, they were initially believed not to play a significant role in the transport of particles. Nonetheless, it was experimentally and numerically evidenced that losses can occur in the presence of these axi-symmetric large scale modes (Fisher *et al.* 2012; Nazikian *et al.* 2008). It was in particular shown that most of these losses are due to chaotic transport in phase-space (Zarzoso *et al.* 2018), but so far so systematic studies of the nature of transport in the presence of EGAMs have been carried out. Similarly, zonal structures can be driven by drift-wave turbulence in magnetized plasmas (Hasegawa *et al.* 1979) and play a major role in the regulation of micro-turbulence induced transport in tokamaks (Lin *et al.* 1998). Although studies of the EP transport in the presence of micro-turbulence have been performed in the past (Angioni *et al.* 2009; Bovet *et al.* 2015; Hauff *et al.* 2009; Pace *et al.* 2013; Zhang *et al.* 2008, 2011), the direct impact of zonal structures on the EP transport remains unexplored. Therefore, we aim in this work to shed light on the fundamental mechanisms responsible for the EP transport in the presence of zonal structures. For this purpose, statistical analyses can be performed to determine some characteristic properties of the transport and the anomalous losses of EP. By *anomalous losses* we mean losses that do not follow the loss rate of a diffusive process. As we will explain, one of the main contributions of this work is to show that these anomalous losses are due to the presence of super-diffusive poloidal transport. In this paper, we focus our analyses on the transport induced by zonal structures in the context of EGAMs, but the results can be extended without any loss of generality to situations where zonal structures are nonlinearly generated by small amplitude perturbations. The remainder of the paper is structured as follows. Section 2 presents the model we use for the statistical analysis. In section 3 we present the observations of fractal-like behaviour and algebraic decay of the exit time of EP using relevant tokamak parameters. This naturally leads to section 4, where we give, for the first time, evidence that zonal structures can lead to anomalous diffusion of energetic particles. Conclusions and future work are presented in section 5.

2. Description of the model

Within the framework of the EGAM-induced transport, we base our analysis on previous results obtained with gyro-kinetic simulations (Zarzoso *et al.* 2018). However, in order to have meaningful statistical analyses, we need to simulate a huge number of test particles during sufficiently long gyro-kinetic simulations. Due to computational restrictions, we avoid this approach by replacing the EGAM potential obtained from the expensive direct gyro-kinetic simulations by an analytical model containing the main physics of the EGAM. This strategy is the most favorable in terms of CPU time, since no interpolation of the field is required. In addition, it allows us to simulate trajectories on time scales comparable with the experimental measurements. The main characteristics of a zonal ($n = 0$) structure are: (1) its frequency, (2) its spatial (radial and poloidal) structure and (3) its amplitude. A zonal structure can therefore be modeled as

$$\phi\left(r, \theta, t\right) \approx \left[\phi_{00}\left(r\right) + \phi_{10}\left(r\right) \sin\theta\right] \cos\left(\omega t\right) \tag{2.1}$$

Based on the ordering $\phi_{10} \sim 10^{-1}\phi_{00}$, we neglect in the following the poloidal dependence and focus only on the dominant component. Following gyro-kinetic simulations (Zarzoso *et al.* 2012, 2013, 2017) we can model the radial dependence as

$$\phi_{00}(r) = \phi_{00}\left(1 - \tanh\left(\frac{r - r_0}{\delta r}\right)\right) \tag{2.2}$$

where ϕ_{00} is the value of the potential at $r = r_0$ and δr controls the width of the mode. This gives a radial electric field of amplitude $E_{r,0} = \phi_{00}/\delta r$ at $r = r_0$ and localised in a region $r_0 - \delta_r/2 < r < r_0 + \delta_r/2$.

The guiding-center equations of motion to be solved in toroidal geometry in the presence of a given electrostatic potential are (Grandgirard *et al.* 2016)

$$\frac{\mathrm{d}x^i}{\mathrm{d}t} = v_\parallel \mathbf{b}^* \cdot \nabla x^i + \mathbf{v}_E \cdot \nabla x^i + \mathbf{v}_D \cdot \nabla x^i \tag{2.3a}$$

$$m_s \frac{\mathrm{d}v_\parallel}{\mathrm{d}t} = -\mu \mathbf{b}^* \cdot \nabla B - eZ_s \mathbf{b}^* \cdot \nabla J_0 \phi + \frac{m_s v_\parallel}{B} \mathbf{v}_E \cdot \nabla B \tag{2.3b}$$

where x^i is the ith contravariant component of the coordinate $\mathbf{x}$ ($x^1 \equiv r$ in the radial direction, $x^2 \equiv \theta$ in the poloidal direction and $x^3 \equiv \varphi$ in the toroidal direction), $v_\parallel$ the parallel component of the velocity along the magnetic field lines, $\mathbf{v}_E$ is the $\mathbf{E} \times \mathbf{B}$ drift, $\mathbf{v}_D$ is the magnetic drift, μ is the magnetic moment, which is an invariant within the present model, m_s is the mass of particles, e is the elementary charge, Z_s is the atomic number, B is the magnitude of the magnetic field, J_0 is the gyro-average operator and $\mathbf{b}^*$ is defined as

$$\mathbf{b}^* = \frac{\mathbf{B}}{B_\parallel^*} + \frac{m_s v_\parallel}{eZ_s B_\parallel^* B} \nabla \times \mathbf{B} \tag{2.4}$$

with

$$B_\parallel^* = B + \frac{m_s}{eZ_s} v_\parallel \mathbf{b} \cdot \nabla \times \mathbf{b} \tag{2.5}$$

where $\mathbf{b}$ is the unit vector along the magnetic field. This expression 2.5 allows us to write the volume element in guiding-centre velocity space as $\frac{2\pi B_\parallel^*}{m_s} \mathrm{d}v_\parallel \mathrm{d}\mu$.

To further reduce the computational time, it is important to realise that due to the axisymmetry of the electrostatic potential, the equation for the toroidal angle does not need to be integrated to determine the radial transport. Axysimmetry also implies the conservation of the toroidal canonical momentum P_φ

$$P_\varphi = -eZ_s \psi + m_s v_\varphi = \text{constant}. \tag{2.6}$$

with $v_\varphi = b_\varphi v_\parallel$, where b_φ is the toroidal covariant component of the unit vector along the magnetic field, R is the major radius and ψ is the poloidal flux, which is written for circular flux surfaces in terms of the safety factor q, the amplitude of the magnetic field at the magnetic axis B_0 and the radial position r as

$$\psi = B_0 \int_0^r \frac{r'}{q(r')} \mathrm{d}r' \tag{2.7}$$

Equation (2.6) allows us to obtain the parallel velocity $v_\parallel$ at each time step without integrating equation (2.3*b*). Finally, for large scale zonal structure the gyro-average is not expected to play a major role. Therefore, we make the simplification $J_0 \cdot \phi = \phi$. This numerical scheme reduces the number of differential equations to be integrated and ensures the exact conservation of the toroidal canonical momentum within machine

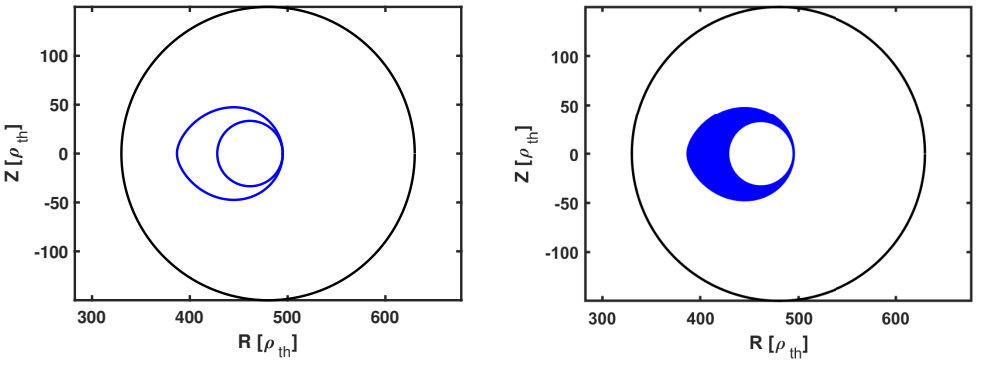

Figure 1: (Left) Trajectories of two counter-passing particles: one deeply counter-passing with ($\Lambda = 0.4, E = 25E_{\rm th}$), represented by the almost circular projection, and one barely counter-passing with ($\Lambda = 0.8, E = 43E_{\rm th}$). (Right) Ensemble of all the possible trajectories with energies within the range $25E_{\rm th} \leqslant E \leqslant 43E_{\rm th}$ and pitch angle $0.4 \leqslant \Lambda \leqslant 0.8$.

precision. The differential equations for r and θ are solved using a $4^{\rm th}$ order Runge-Kutta explicit integration in time. Following a convergence test, the time step for all the simulations has been set up to $\Delta t = 50$ normalized to the cyclotron period. In all the simulations presented in this paper, the safety factor is assumed to be flat and set to $q = 1.8$, the width of the electrostatic potential is $\delta r = 20\rho_{\rm th}$, which is larger than the maximum Larmor radius of the energetic particles that we consider, and the frequency is $\omega = 3.7 \cdot 10^{-3}$ normalized to the cyclotron frequency, which is typical of self-consistent gyro-kinetic simulations presented in (Zarzoso *et al.* 2018).

3. Fractal-like dependence of loss time on initial conditions

Motion invariants are very valuable to describe how the trajectories are modified in the presence of a perturbation. This is because in the absence of any perturbation, a particle initialised with a given value of the invariants will explore the phase-space while keeping the motion invariants constant, which translates into a 1D curve in the 3D real space when two invariants exist. We know that this trajectory will correspond to the one of any other particle initialised in such a way that at $t = 0$ it has the same motion invariants. The unperturbed trajectory of a particle can for instance be described by the kinetic energy E and the ratio between the magnetic moment and the kinetic energy, $\Lambda = \mu B_0/E$, providing the initial radial position is known. An example is illustrated in figure 1, where the left panel represents the projection onto the poloidal cross-section of the trajectories of two particles, one deeply counter-passing and the other barely counter-passing, both starting at the radial position $r/a = 0.1$ and the poloidal angle $\theta = 0$. Of course, particles are injected with a certain range of E and Λ. If all the particles are injected roughly at the same position, the resulting trajectories will cover the area represented by the blue region in the right panel of figure 1.

One can use then the electrostatic potential model in equation (2.1) to study the losses of particles injected in the inner region of the tokamak, at $r/a \approx 0.1$ with a certain range of E and Λ. It is to be noted that the adiabatic invariance of the magnetic

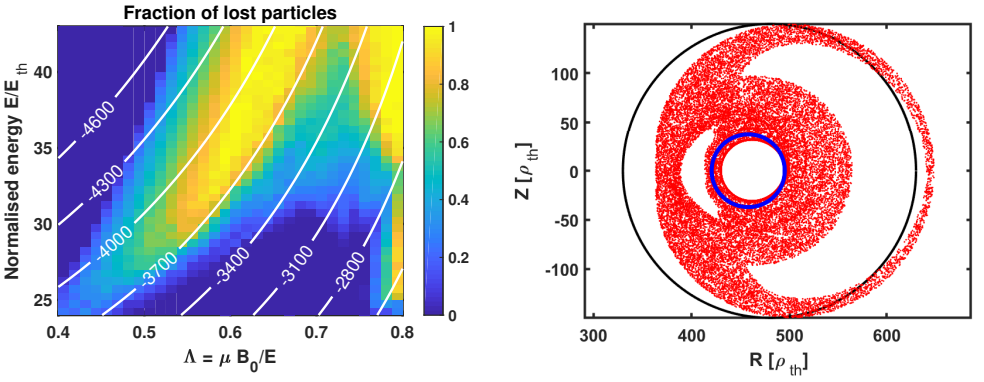

(a) (b)

Figure 2: (Left) Fraction of lost particles as a function of initial E and Λ in the presence of a perturbation. The overlaid contours correspond to P_φ = constant. (Right) Poincaré map of an initial condition with $\Lambda = 0.54$ and $E = 31.5E_{\rm th}$ without perturbation (blue dots) and with perturbation (red dots).

moment μ is imposed owing to the gyro-kinetic ordering. In addition, since the modes are axisymmetric, the toroidal canonical momentum P_φ is an exact invariant, which is also imposed by solving equation 2.6. Regarding the kinetic energy, it remains invariant only if the perturbed potential does not depend explicitly on time. The fact that we have only two motion invariants of guiding-centres in a system with three degrees of freedom makes it actually possible that the motion is chaotic, as reported in (Zarzoso *et al.* 2018). We have performed a set of simulations for each couple (E, Λ) up to $t = 2 \cdot 10^5$ cyclotron periods. The result of this calculation is given in figure 2. The left panel shows the fraction of lost particles as a function of their initial kinetic energy and Λ, with iso-contours of the toroidal canonical momentum.

When focusing on a particular point of figure 2a, (for instance the one with initial $\Lambda = 0.54$ and $E = 31.5E_{\rm th}$, characterised by a lost fraction of roughly 0.8), we can plot the invariant surface in the absence of the perturbation (blue circle) and the Poincaré map in the presence of the perturbation of the particles initialized on that blue circle. This is what figure 2b shows. This is a clear example of how an initially confined counter-passing particle can be lost due to the perturbation. The escape region is given by the intersection of the chaotic sea (red dots) with the tokamak wall (black circle), and depends on the initial conditions of the lost particle.

Figure 2b seems to indicate that all particles initialized on the blue circle should leave the domain, but figure 2a shows that only 80% of the particles are lost. There are two complementary explanations for this issue, one numerical and another theoretical. Numerically, it should be kept in mind that all results pertain finite-time dynamics, which for the simulations reported in figure 2a is $2 \cdot 10^5$ cyclotron periods. That is, figure 2a is the fraction of particles lost at or before $2 \cdot 10^5$ cyclotron periods. There is also a theoretical aspect to this issue related to the fact that the *red region* in figure 2b does not have a trivial topology because (as it is common in Hamiltonian chaos) the Poincaré map of an orbit does not necessarily fill ergodically a simple 2-D manifold Indeed, even if we were able to run a simulation for arbitrarily long time, we might find particles initialized in the blue circle that do not intercept the wall, despite the fact that the blue circle seems to be sort of *embedded* in the *chaotic red region*. There are also boundaries

between the non-chaotic regions (e.g., the *white islands* where the red point did not enter) and the *chaotic region* (i.e., the region that contains the red points in the Poincaré map) separated by Cantor sets known as *Cantori* (see e.g. (Meiss 1992)) that trap particles and preclude them from escaping.

The observed chaotic motion implies that the trajectories of particles exhibit sensitive dependence on initial conditions. It is thus expected that the exit time of the lost particles also exhibits sensitive dependence on initial conditions. Analysing this dependence is especially relevant, since it allows to identify the existence of patterns or structures. This cannot be done with diagrams of lost particles as those reported in (Zarzoso *et al.* 2018), because the quantity plotted there was binary (either the particle is lost or it remains confined). Of course, since the exit time of particles that are never lost is infinite, the best way to represent the exit time is by plotting its inverse, i.e. $t_{\rm exit}^{-1}$. Figure 3 shows the inverse of the exit time as a function of the initial parallel velocity and magnetic moment. The top panel shows $t_{\rm exit}^{-1}$ for all the simulated initial conditions. A clear pattern of structures aligned with the trapping cone is observed. To unveil the detailed structure of the dependence of $t_{\rm exit}^{-1}$ on $v_\parallel$ and μ, the middle and bottom panels show succesive zooms, revealing similar structures at smaller scales when focusing on the region of lost particles. It is to be noted that, although the successive zooms do not exhibit exact self-similarity, it is clear that there is a non-trivial dependence of the exit time on initial conditions at all scales, what we refer to as *fractal-like behaviour*. The observed property of scale invariance imply similarity properties that can be uncovered when performing statistical analysis of the particle dynamics.

We can now focus the analysis on a more restricted region in velocity space, selecting almost mono-energetic EP injected in a localised region of the tokamak and determining the probability distribution function (PDF) of their exit time. We assume experiment-relevant parameters, taking the minor radius of the tokamak (a) and the thermal ion Larmor radius ($\rho_{\rm th}$) such that $\rho_\star = 1/150$, with $\rho_\star = \rho_{\rm th}/a$, and we calculate the exit time of an ensemble of counter-passing EP. Such EP are characteristic of NBI heating in medium-size tokamaks like DIII-D. For this purpose, we follow $\sim 4 \cdot 10^5$ deuterium tracers initialised at the position $r = 0.4a$, $\theta = 0$, $\varphi = 0$, with energy $E \approx 20 E_{\rm th}$ and magnetic moment such that $\mu B_0/T_i = 14$. These particles are confined in the absence of any perturbation. We use GYSELA normalizations (Grandgirard *et al.* 2016), but one can recover the units by choosing parameters for standard tokamaks. For instance, with $T_i \approx 4\,{\rm keV}$ and $B_0 \approx 2\,{\rm T}$, one gets $a \approx 0.67\,m$, which is typical of medium-size tokamaks. Using the amplitude of the EGAM in nonlinear GYSELA simulations ($\phi_{00} = 1.5$), and using the electron temperature $T_e \approx 3\,{\rm keV}$, the amplitude of the radial electric field is $E_{r,0} \approx 14\,{\rm kV \cdot m^{-1}}$, which is of the same order as the one obtained in (Fisher *et al.* 2012). Despite the simple structure of ϕ, its time dependence leads to radial transport and losses. The PDF of the exit time, $\mathcal{P}_{\rm exit}$, is plotted in Fig. 4 in log − log scale, showing an algebraic decay $\mathcal{P}_{\rm exit} \sim t^{-\mu_e}$, in contrast with the exponential decay one would expect in the case of a diffusive transport (Gardiner 2004). For the parameters chosen here, the tail of the PDF is developed from $1 - 100$ ms. It is to be noted that a long time decay was mentioned in (Fisher *et al.* 2012), although no scaling was provided.

To compare with the expected result in the case of diffusive behavior, we can perform a simple exercise where we consider motion of an ensemble of particles initially located at $(x, y) = (0, 0)$ on a 2D disk. The two physical parameters in this simple model are the diffusivity, D, and the radius of the circle, R_c. Figure 5 shows the probability of the exit time for different values of R_c and D according to a Monte-Carlo simulation of the diffusion equation on a disk. For all values of R_c and D the probability exhibits an

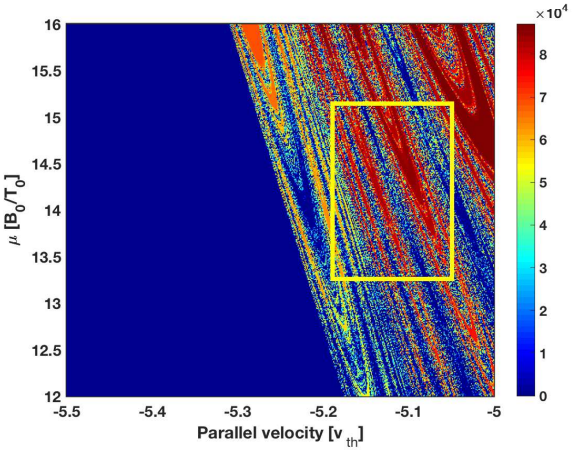

(a)

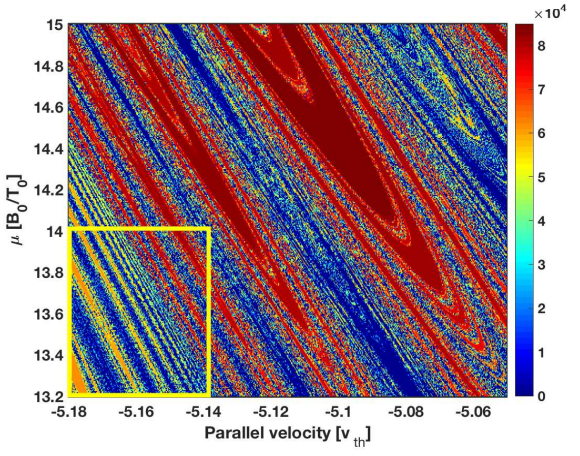

(b)

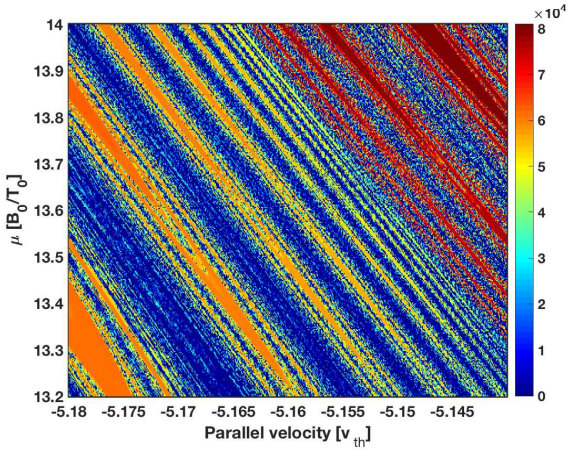

(c)

Figure 3: Inverse of the exit time as a function of the initial parallel velocity and magnetic moment. The middle and bottom panels show succesive zooms of the $(v_\parallel, \mu)$ parameter space, illustrating the same structures at smaller scales.

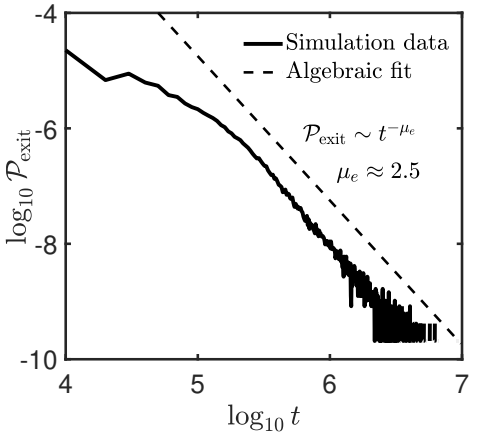

Figure 4: Probability distribution function (PDF) of the exit time for counter-passing EP initialised at $r = 0.4a$, $\theta = 0$, $\varphi = 0$, with $E = 20E_{\rm th}$ and $\mu B_0/T_i = 14$. The dashed line shows an algebraic fit, with $\mu_e = 2.5$.

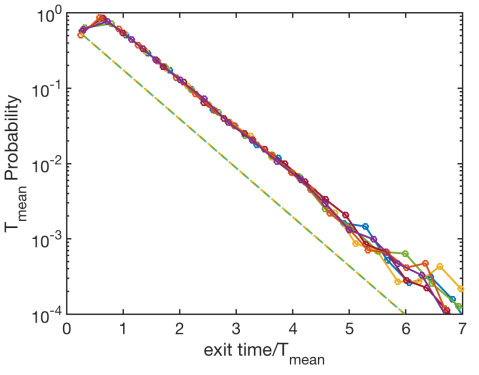

Figure 5: Monte Carlo simulation of exit time for an ensemble of particles initialized at $(x, y) = (0, 0)$ on a disk of radius R_c in the presence of a diffusivity D. The plot shows the probability dependence on time rescaled by the analytical mean exit time $T_{\rm mean}$ in Eq. (3.2) for $(R_c, D) = \{(0.1, 1), (1, 0.1), (1, 10)\,(2, 1)\,(10, 1)\,(1, 1)\}$. The dashed line shows an exponential fit with decay rate $\lambda = 3/2$.

exponential decay of the form

$$P_{diff} \sim T_{\rm mean} \exp\left[-\lambda t/T_{\rm mean}\right] , \tag{3.1}$$

where $\lambda \approx 3/2$ and $T_{\rm mean}$ is the mean exit time (first moment) for particles under the Brownian motion on a disk,

$$T_{\rm mean} = \frac{\pi R_c^2}{4D} . \tag{3.2}$$

It is interesting to point out that, because in figure 4 we get $\mu_e > 2$, the mean exit time does exists. However, the second moment, is infinite and thus not defined. This is in stark contrast with the diffusion problem for which all the moments of the exit time distribution exist.

To understand why this algebraic decay occurs and therefore why the radial transport is not diffusive in the presence of an oscillating radial electric field, we focus on the region responsible for the chaotic transport of particles, i.e. the stochastic layer separating the passing and trapped particles. Let us remind that, in the absence of any perturbation, the particles in a tokamak are divided into trapped and passing and the boundary between these two classes is called trapping cone. This cone is a well defined surface in phase-space, also called separatrix, since it represents the separation between the two classes of particles. The black lines in figure 6 represent the Poincaré map of the unperturbed trajectories for passing and trapped particles. The left panel represents the projection onto the poloidal cross-section, i.e. onto the (R, Z) sub-space, and the right panel represents the projection onto the $\left(r^2/2, \theta\right)$ sub-space. The dashed blue lines with arrows in the left panel indicate the direction of the trajectories of the particles contained in each region. We assume that counter-passing particles are injected in the inner part of the tokamak. Therefore, those particles rotate in the clockwise direction. When they become trapped and eventually co-passing, they rotate in the anti-clockwise direction. This occurs in the outer region of the tokamak, where particles can intercept the wall and be lost. The red region represents the Poincaré map of particles located on the separatrix in the presence of an oscillating radial electric field. It is clearly observed that the separatrix is transformed into a chaotic area connecting the inner and outer parts of the tokamak. More interestingly, it is to be noted that the separation between inner and outer regions is done strictly speaking in the radial direction. Since the radial region that the particle explores when going from one region to another is necessarily bounded by the minor radius of the tokamak, the statistics might be meaningless when focusing on the radial excursion of particles. However, due to the conservation of P_φ, the radial position is intrinsically linked to the parallel velocity, which is in turn linked to the time derivative of the poloidal angle according to Eq. 2.3*a* applied to $i = 2$, corresponding to $x^2 \equiv \theta$. Combining the conservation of P_φ and the time derivative of the poloidal angle, we can write

$$P_\varphi \approx -eZ\psi + m\frac{b_\varphi}{b^\theta}\frac{\mathrm{d}\theta}{\mathrm{d}t} \Rightarrow r^2 \approx \frac{2q}{eZ}\left(-P_\varphi + m\frac{b_\varphi}{b^\theta}\frac{\mathrm{d}\theta}{\mathrm{d}t}\right) \tag{3.3}$$

with P_φ constant and b^θ the poloidal contravariant component of the unit vector along the magnetic field. In other words, when the poloidal angle decreases the counter-passing particle is confined in the core of the tokamak, and when the poloidal angle increases the particle becomes co-passing in the outer region. Contrary to the behaviour of the radial position, the poloidal angle that the particle explores can be arbitrarily large. Therefore, the statistical analysis of the poloidal excursion can be easily done with the possibility to be connected to the radial excursion. In the following, we study only the statistics in the poloidal angle, which exhibits a stochastic behaviour in the presence of the oscillating electric field and so does the radial position.

4. Anomalous exit time and asymmetric diffusion

Our analysis follows closely the one reported in (del Castillo-Negrete 1998) for the transport of passive scalars in vortices in the presence of a shear flow. We follow during $\sim 10^7$ cyclotron periods an ensemble of $\sim 10^5$ energetic particles initialised with $E \approx 20E_{\mathrm{th}}$ in the chaotic region. We calculate their poloidal displacement, defined as

$$\Delta\theta\left(t\right) = \theta\left(t\right) - \theta\left(0\right) \tag{4.1}$$

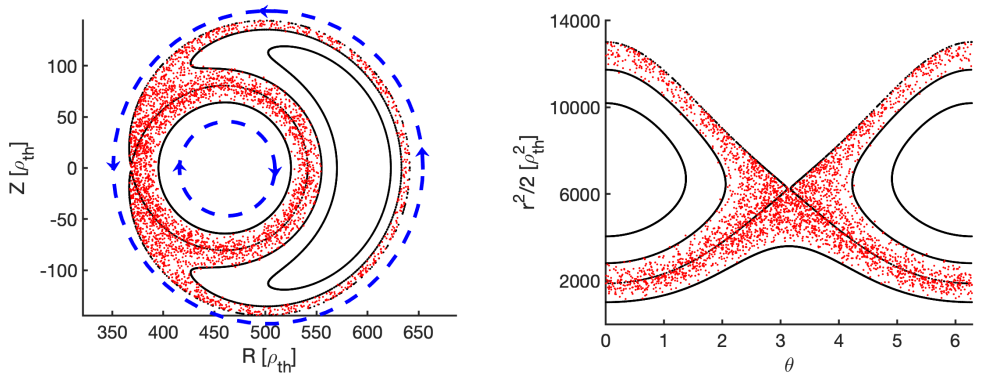

(a) (b)

Figure 6: Poincaré map of unperturbed trajectories (black lines) and particles initialised on the separatrix in the presence of an EGAM (red dots). The direction of rotation of particles in the inner and outer regions of the tokamak is represented by dashed blue lines in the left panel.

which is plotted, for a subset of these particles, in the left panel of figure 7, where a clear spreading is observed. The question arises whether this spreading results from a diffusion in the poloidal direction or not. This can be analysed with the variance of the poloidal displacement, defined as

$$\sigma_\theta^2(t) = \left\langle (\Delta\theta - \langle\Delta\theta\rangle)^2 \right\rangle \tag{4.2}$$

where the time dependence of the poloidal displacement has been dropped for the sake of clarity and the brackets $\langle\cdots\rangle$ represent an ensemble average. When the variance exhibits algebraic growth in time, i.e. $\sigma_\theta^2(t) \sim t^\gamma$, the poloidal transport can be classified as

$\gamma < 1$: sub-diffusive
$\gamma = 1$: diffusive
$1 < \gamma < 2$: super-diffusive
$\gamma = 2$: ballistic

The super- and sub- diffusive regimes correspond to *anomalous diffusion*.

In the right panel of figure 7 we represent by open red symbols the time trace (in $\log - \log$ scale) of the variance of the poloidal displacement as measured from our simulations using the expressions 4.1 and 4.2. The solid red line represents the linear fit in $\log - \log$ scale. For comparison, we also show the ballistic (dotted-dashed black line) ans diffusive (dotted blue line) scalings. It is clear that our simulations are bounded by both processes, meaning that the spreading observed in the left panel is due to a super-diffusion, with an exponent $\gamma = 1.64$. It is to be noted that this super-diffusion occurs in the poloidal direction, not necessarily in the radial direction.

The existence of anomalous diffusion implies that the motion of the guiding-centres cannot be modelled using a diffusion equation, which has important consequences when trying to predict the transport of energetic particles by means of reduced fluid models. As explained in (del Castillo-Negrete 1998), the anomalous diffusion is understood as follows(Lesieur 2008). Let us consider the Lagrangian velocity

$$\frac{\mathrm{d}\Delta\theta}{\mathrm{d}t} = v^\theta(t) \tag{4.3}$$

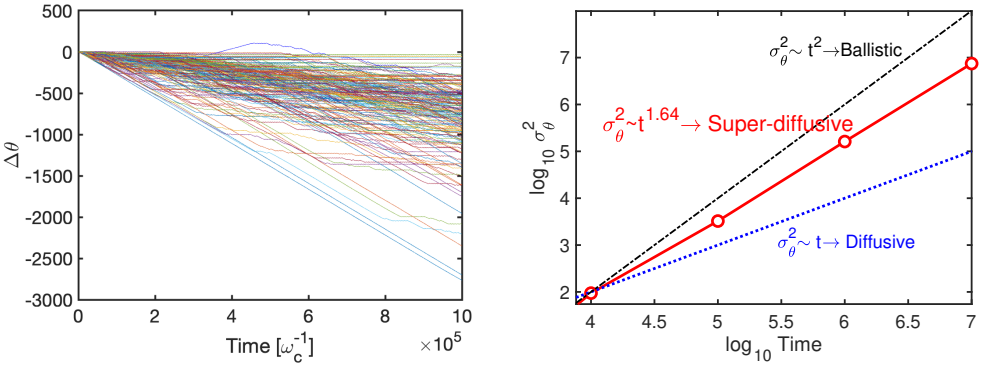

(a) (b)

Figure 7: (Left) Poloidal displacement of passive tracers showing a spreading in the poloidal direction. (Right) Time dependence of the variance of the poloidal displacement.

and the Lagrangian diffusion coefficient

$$\mathcal{K}(t) = \frac{1}{2}\frac{\mathrm{d}}{\mathrm{d}t}\left\langle (\Delta\theta - \langle\Delta\theta\rangle)^2 \right\rangle \tag{4.4}$$

which can simply be expressed as $\mathcal{K}(t) = \int_0^t \left\langle v^\theta(\tau)\, v^\theta(0)\right\rangle \mathrm{d}\tau = \int_0^t \mathcal{C}(\tau)\,\mathrm{d}\tau$. Therefore the time derivative of the variance is expressed in terms of the integral of the Lagrangian velocity auto-correlation function as follows

$$\frac{\mathrm{d}\sigma_\theta^2}{\mathrm{d}t} = 2\int_0^t \mathcal{C}(\tau)\,\mathrm{d}\tau \tag{4.5}$$

Therefore, the scaling of the variance depends on how the Lagrangian velocity auto-correlation function decays in time. If the auto-correlation function decays fast enough in time, the integral 4.5 exists in the limit $t \to \infty$, meaning that $\sigma_\theta^2 \sim t$ and defining the diffusion coefficient $\mathcal{K}$. If the auto-correlation function exhibits an algebraic decay (for $\gamma \neq 1$) as $\mathcal{C} \sim t^{\gamma-2}$, then $\sigma_\theta^2 \sim t^\gamma$. The anomalous diffusion is therefore related to the slow decay of the auto-correlation function. This behaviour is understood in terms of the physics at play. Indeed, an energetic counter-passing particle is injected in the inner region of the tokamak and will remain rotating in the clock-wise direction unless something (the chaotic separatrix) makes it change its radial position until it becomes magnetically trapped. Once it is trapped, the poloidal displacement vanishes on average (there is no transport). The particle will remain trapped unless the chaotic separatrix makes it change again its radial position. It will become either co-passing, evolving as if the particles was *flying* towards positive poloidal angles, or counter-passing, evolving as if the particle was *flying* towards negative poloidal angles. A super-diffusion can therefore be understood as a compromise between trapping periods and short and rare events called *flights*, which tend to de-trapped the particles. More especifically, we interpret the observed super-diffusive transport in the framework of the Continuous Time Random Walk (CTRW) model. The CTRW extends the standard Brownian random walk (which underlies diffusive transport) by allowing non-Gaussian jump distributions and/or non-Markovian waiting time distributions (Metzler & Klafter 2000; Montroll & Weiss 1965), caused by the presence of coherent structures (magnetically trapped and passing regions) which make particles spend an anomalous amount of time moving slowly (trapping

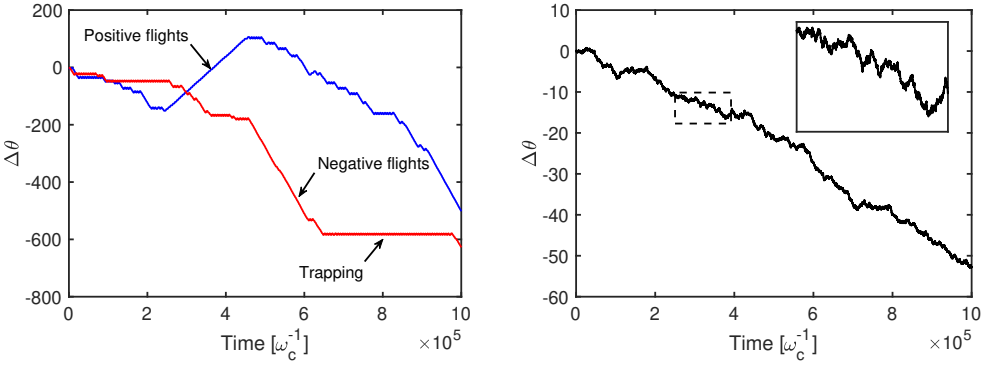

Figure 8: (Left) Poloidal displacement of two passive tracers, showing the existence of positive and negative flights. (Right) Poloidal displacement assuming an asymmetric random walk.

region) or fast (passing region) (del Castillo-Negrete 1998), the bridge between both being ensured by the chaotic separatrix. Of particular interest to this work is the case of Lévy flights which are jumps with diverging second moments.

The existence of the flights is clearly visible in the left panel of figure 8, where we plot the poloidal displacement of two tracers during the first 10^6 cyclotron periods. It can be observed that sometimes the particle is magnetically trapped and therefore the poloidal displacement does not evolve on average. Sometimes, there are either positive or negative flights which de-trap the particles. As a comparison, we give in the right panel of the figure a time trace assuming an asymmetric standard random walk, in the absence of any flights.

Coming back to figure 6, when an EP becomes trapped it is lost if the wall of the tokamak intercepts the chaotic region, which is the case here since $a = 150\rho_{\rm th}$. The exit time of a counter-passing particle is related to the time a particle spends moving towards negative poloidal angles, since the particle remains in the inner region of the tokamak. Accordingly, the probability distribution function (PDF) of the exit time, $\mathcal{P}_{\rm exit}$, corresponds to the PDF of the negative flights of duration t, $\mathcal{P}^-_{\rm flight}$, i.e.

$$\mathcal{P}_{\rm exit} \equiv \mathcal{P}\left(t_{\rm exit} = t\right) = \mathcal{P}^-_{\rm flight}\left(t\right) \tag{4.6}$$

To verify this connection, figure 9 shows the probability distribution function (PDF) of negative (left panel) and positive (right panel) flights of duration t. As expected, the PDF of negative flights exhibits an algebraic decay, $\mathcal{P}^-_{\rm flight} \sim t^{-\mu_f}$, with $\mu_f \approx \mu_e$, where as shown in Fig. 4 $\mathcal{P}_{\rm exit} \sim t^{-\mu_e}$. The PDF of positive flights decays faster, following an exponential scaling ($\mathcal{P}^-_{\rm flight} \sim {\rm e}^{-\lambda t}$). This finding has a physical impact in terms of radial transport: a counter-passing particle spends, probabilistically speaking, more time in the inner region than a co-passing particle in the outer region. This leads to an asymmetrically poloidal (and therefore radial) transport in the presence of the chaotic separatrix. Note that, because $\mu_f < 3$, the second moment of the PDF of negative flights diverges, $\int_0^\infty t^2 \mathcal{P}^-_{\rm flight} {\rm d}t \to \infty$. That is, the negative flights are Lévy flights which invalidates the use of the central limit theorem (CLT) as it is customary done in the Brownian random walk model of diffusive transport. On the other hand, within the

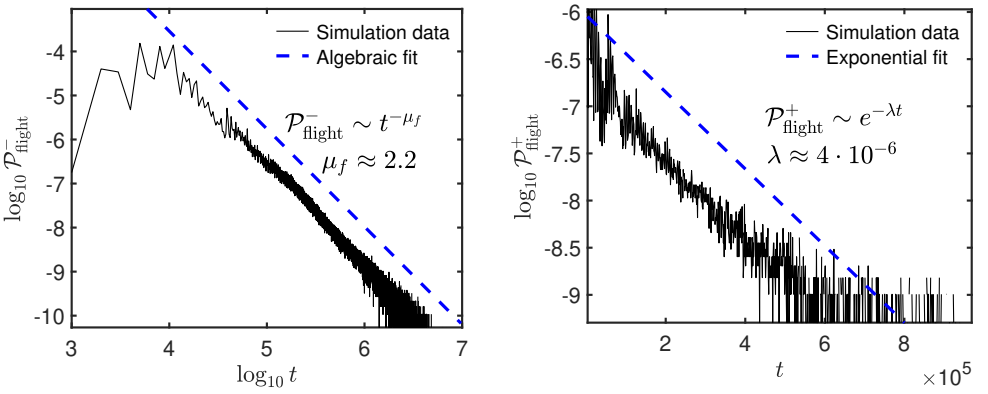

(a) (b)

Figure 9: PDF of negative (left) and positive (right) flight events of duration t.

CTRW, superdiffusive behavior, $\gamma > 1$, is a natural consequence of the existence of Lévy flights, $\mu_f < 3$. In particular, according to CTRW theory $\gamma = 2/(\mu_f - 1)$ which for the numerically determined exponent $\mu_f \approx 2.2$ predicts $\gamma = 1.66$, a value very close to the numerically observed $\gamma \approx 1.64$. Let us remind that the theory of the Brownian motion relies upon the application of the CLT, which states that the sum of N i.i.d. random variables $\{x_i\}_{1 \leqslant i \leqslant N}$ is described by a Gaussian distribution in the limit $N \to \infty$, as long as the first and second moments exist, i.e. $\langle x_i \rangle < \infty$ and $\langle x_i^2 \rangle < \infty$. One can naturally ask what happens in the case where one of the moments (or even both) does not exist, which is our case. Fortunately, there is a generalization of the CLT for this kind of situations, which was formulated by P. Lévy in the 1930s. The Gaussian distribution function as limit of the sum of i.i.d. variables is replaced by the so-called Lévy or *α-stable distribution*, characterised by long heavy tails and diverging moments (see for instance (Lévy 1934, 1940) and references therein).

Back to our physical problem, figure 10 shows the PDF of the total (summed) poloidal displacements at different times as a function of the similarity variable

$$\chi = \frac{\Delta\theta - \langle \Delta\theta \rangle}{t^{\gamma/2}} \tag{4.7}$$

The definition of this variable is not a coincidence. Indeed, the collapse of the rescaled PDFs at different times provides numerical evidence that poloidal transport exhibits self-similar dynamics with anomalous exponent γ which, consistent with the CTRW model, is equal to the numerically determined super-diffusive exponent $\gamma \approx 1.64$. Formally, the observed self-similar evolution implies the existence of a scaling function F satisfying $\mathcal{P}_{\Delta\theta} = t^{-\gamma/2} F(\chi)$.

It is observed that the scaling function departs significantly from a Gaussian distribution (represented by a dashed grey line for comparison, which is representative of diffusive processes). Also, the asymmetry in the flights is reflected in the asymmetry of the scaling function. Moreover, according to the CTRW, it should exhibit an algebraic decay of the $\chi < 0$ tail of the form $F \sim \chi^{-(\alpha^- + 1)}$ with $\alpha^- = \mu_f - 1$, a results fully consistent with the numerically obtained values $\mu_f \approx 2.2$ and $\alpha^- \approx 1.2$. For the $\chi > 0$ tail, within the CTRW, the exponential decay of $\mathcal{P}^+_{flight}$ implies, consistent with the numerical results,

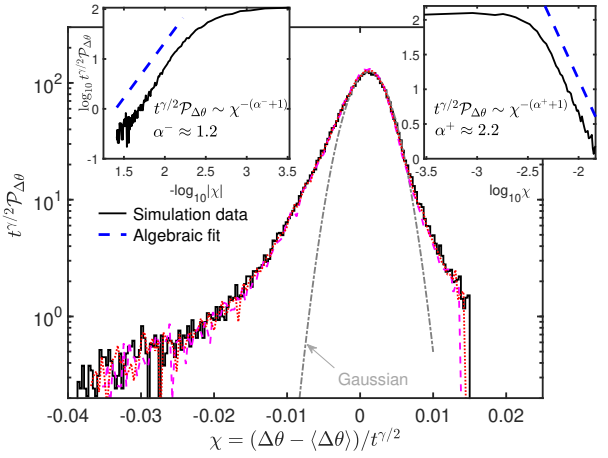

Figure 10: Rescaled PDF of poloidal displacements at different times: $\omega_c t = 9{\cdot}10^6$ (dashed magenta), $\omega_c t = 9.5 \cdot 10^6$ (dotted red) and $\omega_c t = 10^7$ (solid black). The dotted-dashed grey line corresponds to a Gaussian PDF. The insets represent the log-log plots of the tails, showing the asymmetric algebraic decays.

$\alpha^+ > 2$. This is represented in the insets of figure 10 showing the log-log plots of the tails of the PDF.

5. Conclusions and future work

In this paper, we have explored the fundamental mechanism of the transport of energetic particles in the presence of an oscillating radial electric field in axi-symmetric tokamak magnetic equilibria. Such scenarios can be found in the presence of EGAMs, for instance Fisher *et al.* (2012); Nazikian *et al.* (2008); Zarzoso *et al.* (2018). We show in particular that initially integrable orbits are transformed into chaotic regions that can intercept the wall of the tokamak, leading to losses of energetic particles. We have provided numerical evidence of fractal-like patterns and anomalous exit time statistics of EP, exhibiting algebraic decay in sharp contrast with the expected exponential exit time in the case of radial diffusive transport. We have shown that the algebraic loss time decay is the result of Lévy flights that lead to super-diffusive poloidal transport and an asymmetric non-Gaussian (Lévy) PDF of displacements. Since the radial displacement is related to the sign of the time derivative of the poloidal angle, the observed poloidal displacement asymmetry translates into a radial displacement asymmetry and energetic particles can spend probabilistically speaking more time in the inner region of the tokamak than in the outer one. These results might have an important impact on the confinement time of EP needed to achieve sustained fusion in burning plasmas, in addition to the potential generation of a toroidal net torque resulting from the poloidal asymmetry of the particle displacements.

The work presented in this paper opens the doors to further analyses that have not been addressed here. First, the observed anomalous radial transport should be quantified in the presence of other mechanisms that could be responsible of diffusive transport. Second, the dependence of the transport (diffusive, super- or sub-diffusive) on the parameters characterizing the oscillating radial electric field should be studied in detail. Third, quantifying the generation of mometum due to the radial asymmetric displacement is

essential in order to assess its effect in future plasma scenarios. Finally, it is known that fractional diffusion results from the continuum (fluid) limit of the (kinetic) CTRW model, see e.g. (del Castillo-Negrete *et al.* 2004; Metzler & Klafter 2000). Accordingly, the observed self-similar dynamics of the PDF of poloidal displacements, along with the consistency of the numerically determined anomalous exponents μ_e, γ, μ_f, α^- and α^+ with the CTRW predictions, opens the possibility to describe EP transport using non-local transport models based on fractional derivatives (del Castillo-Negrete 2006). These four directions of research will be explored in a forthcoming publication.

6. Acknowledgments

D.dCN was sponsored by the Oak Ridge National Laboratory, managed by UT-Battelle, LLC, for the US Department of Energy under Contract No. DE-AC05-00OR22725

REFERENCES

Angioni, Clemente, Peeters, AG, Pereverzev, GV, Bottino, Alberto, Candy, J, Dux, Ralph, Fable, Emiliano, Hein, T, & Waltz, RE. 2009. Gyrokinetic simulations of impurity, He ash and α particle transport and consequences on ITER transport modelling. *Nuclear Fusion*, **49**(5), 055013.

Bovet, A, Fasoli, A, Ricci, P, Furno, I, & Gustafson, K. 2015. Nondiffusive transport regimes for suprathermal ions in turbulent plasmas. *Physical Review E*, **91**(4), 041101.

Chen, L., & Zonca, F. 2007. Theory of Alfvén waves and energetic particle physics in burning plasmas. *Nuclear Fusion*, **47**, S727.

Chen, Liu, & Zonca, Fulvio. 2012. Nonlinear Excitations of Zonal Structures by Toroidal Alfvén Eigenmodes. *Phys. Rev. Lett.*, **109**(Oct), 145002.

Chen, Liu, & Zonca, Fulvio. 2016. Physics of Alfvén waves and energetic particles in burning plasmas. *Reviews of Modern Physics*, **88**(1), 015008.

del Castillo-Negrete, D. 1998. Asymmetric transport and non-Gaussian statistics of passive scalars in vortices in shear. *Physics of Fluids*, **10**(3), 576–594.

del Castillo-Negrete, Diego. 2006. Fractional diffusion models of nonlocal transport. *Physics of plasmas*, **13**(8), 082308.

del Castillo-Negrete, Diego, Carreras, BA, & Lynch, VE. 2004. Fractional diffusion in plasma turbulence. *Physics of Plasmas*, **11**(8), 3854–3864.

Fisher, RK, Pace, DC, Kramer, GJ, Van Zeeland, MA, Nazikian, R, Heidbrink, WW, & García-Muñoz, M. 2012. Beam ion losses due to energetic particle geodesic acoustic modes. *Nuclear Fusion*, **52**(12), 123015.

Fu, GY. 2008. Energetic-Particle-Induced Geodesic Acoustic Mode. *Physical review letters*, **101**(18), 185002.

Gardiner, C. W. 2004. *Handbook of stochastic methods*. Springer Verlag.

Grandgirard, Virginie, Abiteboul, Jérémie, Bigot, Julien, Cartier-Michaud, Thomas, Crouseilles, Nicolas, Dif-Pradalier, Guilhem, Ehrlacher, Ch, Esteve, Damien, Garbet, Xavier, Ghendrih, Ph, *et al.* 2016. A 5D gyrokinetic full-f global semi-lagrangian code for flux-driven ion turbulence simulations. *Computer Physics Communications*, **207**, 35–68.

Hasegawa, Akira, Maclennan, Carol G, & Kodama, Yuji. 1979. Nonlinear behavior and turbulence spectra of drift waves and Rossby waves. *The Physics of Fluids*, **22**(11), 2122–2129.

Hauff, T, Pueschel, MJ, Dannert, T, & Jenko, F. 2009. Electrostatic and magnetic transport of energetic ions in turbulent plasmas. *Physical Review Letters*, **102**(7), 075004.

Heidbrink, WW. 2008. Basic physics of Alfvén instabilities driven by energetic particles in toroidally confined plasmas. *Physics of Plasmas*, **15**(5), 055501.

Heidbrink, WW, & Sadler, GJ. 1994. The behaviour of fast ions in tokamak experiments. *Nuclear Fusion*, **34**(4), 535.

Lauber, Philipp. 2013. Super–thermal particles in hot plasmas–Kinetic models, numerical

solution strategies, and comparison to tokamak experiments. *Physics Reports*, **533**(2), 33–68.

Lesieur, Marcel. 2008. *Turbulence in Fluids*. Springer.

Lévy, Paul. 1934. Sur les intégrales dont les éléments sont des variables aléatoires indépendantes. *Annali della Scuola Normale Superiore di Pisa-Classe di Scienze*, **3**(3-4), 337–366.

Lévy, Paul. 1940. Sur certains processus stochastiques homogènes. *Compositio mathematica*, **7**, 283–339.

Lin, Zhihong, Hahm, Taik Soo, Lee, WW, Tang, William M, & White, Roscoe B. 1998. Turbulent transport reduction by zonal flows: Massively parallel simulations. *Science*, **281**(5384), 1835–1837.

Meiss, JD. 1992. Symplectic maps, variational principles, and transport. *Reviews of Modern Physics*, **64**(3), 795.

Metzler, Ralf, & Klafter, Joseph. 2000. The random walk's guide to anomalous diffusion: a fractional dynamics approach. *Physics reports*, **339**(1), 1–77.

Montroll, Elliott W, & Weiss, George H. 1965. Random walks on lattices. II. *Journal of Mathematical Physics*, **6**(2), 167–181.

Nazikian, R., Fu, GY, Austin, ME, Berk, HL, Budny, RV, Gorelenkov, NN, Heidbrink, WW, Holcomb, CT, Kramer, GJ, McKee, GR, *et al.* 2008. Intense geodesic acousticlike modes driven by suprathermal ions in a tokamak plasma. *Physical review letters*, **101**(18), 185001.

Pace, DC, Austin, Max E, Bass, EM, Budny, RV, Heidbrink, WW, Hillesheim, JC, Holcomb, CT, Gorelenkova, M, Grierson, BA, McCune, DC, *et al.* 2013. Energetic ion transport by microturbulence is insignificant in tokamaks. *Physics of Plasmas*, **20**(5), 056108.

Pinches, SD, Berk, HL, Borba, DN, Breizman, BN, Briguglio, S, Fasoli, A, Fogaccia, G, Gryaznevich, MP, Kiptily, V, Mantsinen, MJ, *et al.* 2004. The role of energetic particles in fusion plasmas. *Plasma physics and controlled fusion*, **46**(12B), B187.

Qiu, Z., Zonca, F., & Chen, L. 2010. *Plasma Physics and Controlled Fusion*, **52**, 095003.

Sharapov, SE, Alper, B, Borba, D, Eriksson, L-G, Fasoli, A, Gill, RD, Gondhalekar, A, Gormezano, C, Heeter, RF, Huysmans, GTA, *et al.* 2000. Energetic particle physics in JET. *Nuclear Fusion*, **40**(7), 1363.

Zarzoso, D., Garbet, X., Sarazin, Y., Dumont, R., & Grandgirard, V. 2012. Fully kinetic description of the linear excitation and nonlinear saturation of fast-ion-driven geodesic acoustic mode instability. *Physics of Plasmas*, **19**(2), 022102–022102.

Zarzoso, D, Sarazin, Y, Garbet, X, Dumont, R, Strugarek, A, Abiteboul, J, Cartier-Michaud, T, Dif-Pradalier, G, Ghendrih, Ph, Grandgirard, V, *et al.* 2013. *Physical Review Letters*, **110**(12), 125002.

Zarzoso, D, Migliano, P, Grandgirard, V, Latu, G, & Passeron, C. 2017. *Nucl. Fusion*, **57**(072011), 072011.

Zarzoso, David, del Castillo-Negrete, D, Escande, DF, Sarazin, Y, Garbet, X, Grandgirard, V, Passeron, C, Latu, G, & Benkadda, S. 2018. Particle transport due to energetic-particle-driven geodesic acoustic modes. *Nuclear Fusion*, **58**(10), 106030.

Zhang, Wenlu, Lin, Zhihong, Chen, Liu, *et al.* 2008. Transport of energetic particles by microturbulence in magnetized plasmas. *Physical review letters*, **101**(9), 095001.

Zhang, Wenlu, Lin, Zhihong, & Chen, Liu. 2011. Comment on "Electrostatic and magnetic transport of energetic ions in turbulent plasmas". *Physical review letters*, **107**(23), 239501.